

# Room Temperature Lasing of InAs/GaAs Quantum Dots in the Whispering Gallery Modes of a Silica Microsphere

Sébastien Steiner<sup>1</sup>, Jean Hare<sup>1</sup>, Valérie Lefèvre-Séguin<sup>1</sup>,  
Jean-Michel Gérard<sup>2</sup>

<sup>1</sup> École normale supérieure – Laboratoire Kastler Brossel  
24 rue Lhomond – 75231 Paris cedex 05 – France

<sup>2</sup> CEA/DRFMC/SP2M -Nanophysics and Semiconductor Laboratory  
17 rue des Martyrs – 38054 Grenoble Cedex – France

[Jean.Hare@lkb.ens.fr](mailto:Jean.Hare@lkb.ens.fr)

**Abstract:** We have achieved low threshold lasing of self-assembled InAs/GaAs quantum dots coupled to the evanescent wave of the high- $Q$  whispering gallery modes of a silica microsphere. In spite of high temperature and  $Q$ -spoiling of WGM due to diffusion and refraction on the high index semiconductor sample, room temperature lasing is obtained with less than 100 quantum dots.

© 2019 Optical Society of America

**OCIS codes:** 130.3120, 140.3410, 140.5960, 160.6030, 270.5580

---

## References and links

1. R. J. Warburton, C. S. Dürr, K. Karrai, J. P. Kotthaus, G. Medeiros-Ribeiro, and P. M. Petroff, “Charged Excitons in Self-Assembled Semiconductor Quantum Dots,” *Phys. Rev. Lett.* **79**, 5282–5285 (1997).
2. J. Marzin, J. Gérard, A. Izraël, D. Barrier, and G. Bastard, “Photoluminescence of Single InAs Quantum Dots Obtained by Self-Organized Growth on GaAs,” *Phys. Rev. Lett.* **73**, 716 (1994).
3. M. Bayer and A. Forchel, “Temperature Dependence of the Exciton Homogeneous Linewidth in  $\text{In}_{0.60}\text{Ga}_{0.40}\text{As}/\text{GaAs}$  Self-Assembled Quantum Dots,” *Phys. Rev. B* **65**, R041,308 (2002).
4. C. Kammerer, C. Voisin, G. Cassabois, C. Delalande, P. Roussignol, F. Klopf, J. P. Reithmaier, A. Forchel, and J. M. Gérard, “Line Narrowing in Single Semiconductor Quantum Dots: Toward the Control of Environment Effects,” *Phys. Rev. B* **66**, R041,306 (2002).
5. P. Borri, W. Langbein, S. Schneider, U. Woggon, R. L. Sellin, D. Ouyang, and D. Bimberg, “Ultralong Dephasing Time in InGaAs Quantum Dots,” *Phys. Rev. Lett.* **87**, 157,401 (2001).
6. S. Haroche, “Cavity Quantum Electrodynamics,” in *Fundamental Systems in Quantum Optics*, J. Dalibard, J. Raimond, and J. Zinn-Justin, eds., Les Houches Summer School, Session LIII (North Holland, 1992).
7. J.-M. Gérard, *Solid-State Cavity-Quantum Electrodynamics with Self-Assembled Quantum Dots*, vol. 90 of *Topics in Applied Physics*, pp. 269 – 314 (Springer, Berlin / Heidelberg, 2003).
8. J. M. Gérard, B. Sermage, B. Gayral, B. Legrand, E. Costard, and V. Thierry-Mieg, “Enhanced Spontaneous Emission by Quantum Boxes in a Monolithic Optical Microcavity,” *Phys. Rev. Lett.* **81**, 1110–1113 (1998).
9. E. Moreau, I. Robert, J. M. Gérard, I. Abram, L. Manin, and V. Thierry-Mieg, “Single-Mode Solid-State Single Photon Source Based on Isolated Quantum Dots in Pillar Microcavities,” *Appl. Phys. Lett.* **79**, 2865 (2001).
10. C. Santori, D. Fattal, J. Vučković, G. S. Solomon, and Y. Yamamoto, “Indistinguishable Photons from a Single-Photon Device,” *Nature* **419**, 594 (2002).
11. D. Englund, D. Fattal, EdoWaks, G. Solomon, B. Zhang, T. Nakao, Y. Arakawa, Y. Yamamoto, and J. Vučković, “Controlling the Spontaneous Emission Rate of Single Quantum Dots in a Two-Dimensional Photonic Crystal,” *Phys. Rev. Lett.* **95**, 013,904 (2005).
12. J. P. Reithmaier, G. Sek, A. Löffler, C. Hofmann, S. Kuhn, S. Reitzenstein, L. V. Keldysh, V. D. Kulakovskii, T. L. Reinecke, and A. Forchel, “Strong Coupling in a Single Quantum Dot–Semiconductor Microcavity System,” *Nature* **432**, 197 (2004).

13. T. Yoshie, A. Scherer, J. Hendrickson, G. Khitrova, H. M. Gibbs, G. Rupper, C. Ell, O. B. Shchekin, and D. G. Deppe, “Vacuum Rabi Splitting with a Single Quantum Dot in a Photonic Crystal Nanocavity,” *Nature* **432**, 200 (2004).
14. E. Peter, P. Senellart, D. Martrou, A. Lemaître, J. Hours, J. M. Gérard, and J. Bloch, “Exciton Photon Strong-Coupling Regime for a Single Quantum Dot Embedded in a Microcavity,” *Phys. Rev. Lett.* **95**, 067401 (2005).
15. K. Srinivasan, M. Borselli, T. J. Johnson, P. E. Barclay, O. Painter, A. Stintz, and S. Krishna, “Optical Loss and Lasing Characteristics of High-Quality-Factor AlGaAs Microdisk Resonators with Embedded Quantum Dots,” *Appl. Phys. Lett.* **86**, 151,106 (2005).
16. B.-S. Song, S. Noda, T. Asano, and Y. Akahane, “Ultra-High-Q Photonic Double-Heterostructure Nanocavity,” *Nat. Mat.* **4**, 207–210 (2005).
17. V. B. Braginsky, M. L. Gorodetsky, and V. S. Ilchenko, “Quality-factor and non-linear properties of optical whispering-gallery modes,” *Phys. Lett. A* **137**, 393–397 (1989).
18. L. Collot, V. Lefèvre-Seguin, M. Brune, J. M. Raimond, and S. Haroche, “Very high-Q whispering-gallery mode resonances observed on fused silica microspheres,” *Europhys. Lett.* **23**, 327 (1993).
19. D. K. Armani, T. J. Kippenberg, S. M. Spillane, and K. J. Vahala, “Ultra-High-*Q* Toroid Microcavity on a Chip,” *Nature* **421**, 925 (2003).
20. V. Sandoghdar, F. Treussart, J. Hare, V. Lefèvre-Seguin, J.-M. Raimond, and S. Haroche, “Very low threshold whispering-gallery mode microsphere laser,” *Phys. Rev. A* **54**, R1777 (1996).
21. W. von Klitzing, E. Jahier, R. Long, F. Lissillour, V. Lefèvre-Seguin, J. Hare, J.-M. Raimond, and S. Haroche, “Very Low Threshold Lasing in Er<sup>3+</sup> Doped ZBLAN Microsphere,” *Electr. Lett.* **35**(20), 1745–1746 (1999).
22. F. Lissillour, P. Feron, N. Dubreuil, P. Dupriez, M. Poulain, and G. M. Stephan, “Erbium-Doped Microspherical Lasers at 1.56  $\mu$ m,” *Electr. Lett.* **36**, 1382–1384 (2000).
23. M. Cai, O. Painter, K. J. Vahala, and P. C. Sercel, “Fiber-Coupled Microsphere Laser,” *Opt. Lett.* **25**, 1430 (2000).
24. L. Yang, D. K. Armani, and K. J. Vahala, “Fiber-Coupled Erbium Microlasers on a Chip,” *Appl. Phys. Lett.* **83**, 825–827 (2003).
25. I. Protsenko, P. Domokos, V. Lefèvre-Seguin, J. Hare, J.-M. Raimond, and L. Davidovich, “Quantum Theory of a Thresholdless Laser,” *Phys. Rev. A* **59**, 1667–1682 (1999).
26. M. Pelton and Y. Yamamoto, “Ultralow Threshold Laser Using a Single Quantum Dot and a Microsphere Cavity,” *Phys. Rev. A* **59**, 2418–2421 (1999).
27. J. C. Knight, N. Dubreuil, V. Sandoghdar, J. Hare, V. Lefèvre-Seguin, J.-M. Raimond, and S. Haroche, “Mapping whispering-gallery modes in microspheres using a near-field probe,” *Opt. Lett.* **20**, 1515 (1995).
28. P. Borri, W. Langbein, J. Mořík, J. M. Hvam, F. Heinrichsdorff, M.-H. Mao, and D. Bimberg, “Dephasing in InAs/GaAs Quantum Dots,” *Phys. Rev. B* **60**, 7784 (1999).
29. F.-M. Treussart, “Étude expérimentale de l’effet Laser dans des microsphères de silice dopées avec des ions néodyme,” Ph.D. thesis, Université Paris VI (1997).
30. S. Steiner, “Microsphères de silice et Boîtes quantiques InAs/GaAs: réalisation d’un microlaser à faible seuil,” Ph.D. thesis, Université Paris VI (2003).
31. Even at 778 nm the large imaginary part of  $N_D \approx 3.67 + i 0.29$  gives  $r \approx -0.78 + i 0.54$ , leading to the same conclusion.
32. The small increase of the coupling efficiency on each side of the central drop indicates the crossing of critical coupling for prim-sphere interaction, initially over-coupled.

---

## 1. Introduction

Semiconductor nanostructures providing efficient confinement of charge carriers have attracted an ever growing interest for several decades. Advances in semiconductor technology have allowed for the fabrication of heterostructures where bandgap discontinuities provide a binding potential in one or several dimensions. The resulting density of states is “engineered” to provide a stronger coupling to the electromagnetic field, favorable for ever more efficient light sources. In epitaxially grown quantum dots (QDs) especially, the 3D confinement leads to the formation of “atom like” discrete levels, thus concentrating oscillator strength on discrete transitions, favoring efficient atom-light interaction. Though significant departures from a truly atom-like system have been characterized, the large oscillator strength associated with the fundamental optical transition makes QDs very promising elementary emitters for both classical and quantum light emitting devices. This transition is characterized by an optical dipole moment in excess of 10 a.u. (1 a.u. =  $ea_0$ ) [1], significantly greater than for atoms or ions, and by a moderate homogeneous broadening (down to below 1 GHz) [2, 3, 4, 5], at least at cryogenic temperatures.

QDs are therefore perfectly suited for solid-state Cavity quantum electrodynamics (CQED) experiments [6], aimed at controlling spontaneous and stimulated emission properties of electron-hole pairs by electromagnetic-mode engineering [7]. In order to enhance matter–field interaction one needs microcavities with small volume modes and high quality factors. Up to now, this has been done by embedding the QDs in semiconductor microcavities which can be a micropillar, a microdisk, or a photonic bandgap cavity. The main interest of semiconductor microcavities resides in the very small mode volumes which can be achieved. Most basic CQED effects have now been observed for QDs in semiconductor cavities, including spontaneous emission rate enhancement [8, 9, 10] or inhibition [11] as well as vacuum Rabi flopping for single QDs [12, 13, 14]. Although quality factors as large as 300,000 have been reported for empty microdisks [15] or photonic crystal cavities [16], reported values are until now significantly smaller for active semiconductor microcavities containing QDs ( $Q < 30,000$ ).

In this context, an interesting alternative is the use of fused silica microspheres [17, 18] or microtoroids [19] sustaining small volume whispering-gallery modes (WGM) with ultrahigh quality factors resulting from high transparency and very small residual roughness. In microspheres, the WGM are formed by successive total internal reflection along the sphere equator leading for a typical sphere of 100  $\mu\text{m}$  in diameter to mode volumes in the range of 1000  $\mu\text{m}^3$  and to a quality factor  $Q$  as high as 10<sup>10</sup> [17, 18].

This unique property is particularly attractive in the context of microlaser physics. Very low-threshold (0.2  $\mu\text{W}$ ) optically pumped lasers have for instance been demonstrated for microspheres or microtoroids doped with rare-earth ions [20, 21, 22, 23, 24]. Such ultralow-loss cavities offer the unique opportunity to reduce the number of active emitters in a laser down to its ultimate limit [25]. A lasing threshold as low as 10 pA has been predicted for a microsphere coupled to a single self-assembled QD [26]. Although such a laser would only work at low temperature [7], it is obviously a very attractive model system to study experimentally the very peculiar physics of single “atom” lasers, in a solid-state system.

In this letter, we report for the first time the laser operation of an original combination of a silica microsphere and few InAs/GaAs self-organized QDs used as the amplifier medium. We had to overcome two challenging problems: the poor radiative efficiency of the QDs at room temperature resulting from thermal promotion of carriers to the continuum states of the wetting layer, and the strong broadening of WGMs induced by the high refractive index sample. Despite these difficulties, we nevertheless achieved a cw laser effect with thresholds as low as 200  $\mu\text{W}$  in absorbed pump power.

## 2. Principle of experiment

### 2.1. Main features of Microsphere WGMs

The high- $Q$  WGM of a silica microsphere of radius  $a \sim 10 - 100 \mu\text{m}$  and refractive index  $N \approx 1.45$  are described, beside TE or TM polarization, by 3 integer numbers  $n, \ell, m$  characterizing the electric field distribution  $E \propto f_{n\ell}(r)Y_\ell^m(\theta, \phi)$ , where  $(r, \theta, \phi)$  are the spherical coordinates. While  $n$  is the number of antinodes of the radial function  $f_{n\ell}(r)$ ,  $\ell$  and  $m$  are the usual angular “quantum” numbers, associated to  $\ell - |m| + 1$  anti-nodes in the polar direction, as experimentally observed in Ref. [27]. The modes with  $n = 1$  and  $|m| = \ell$  are confined at the wavelength scale around the sphere equator, with an evanescent wave in the surrounding air medium roughly decaying as  $\exp(-\kappa r)$ , where  $\kappa \approx (N_{\text{eff}}^2 - 1)^{1/2} 2\pi/\lambda$ , with  $N_{\text{eff}} = \ell\lambda/2\pi a$  the WGM’s effective index, close to the refractive index of silica  $N$ .

The WGM verify the approximate relation  $2\pi a \approx \ell\lambda/N$ , and this results in a quasi periodic spectrum with an effective free spectral range (FSR)  $\Delta\nu_{\text{FSR}} \approx c/2\pi Na$ .

Due to a small ellipticity, the WGM differing only in  $|m|$  exhibit different resonance frequencies. In a given FSR, frequency scanning combined with appropriate beam settings allows us to

excite modes of various  $n$  or  $\ell - |m|$ , which can be identified by spectroscopic methods.

## 2.2. QD Sample

We used a sample containing InAs/GaAs QDs grown by molecular beam epitaxy on a (001) GaAs substrate. The epitaxial structure consisted in a 500 nm thick GaAs buffer layer, 30 nm  $\text{Al}_{0.15}\text{Ga}_{0.85}\text{As}$ , 50 nm GaAs, a layer of InAs QDs, 20 nm GaAs, 10 nm  $\text{Al}_{0.15}\text{Ga}_{0.85}\text{As}$ , and on top a 2.1 nm GaAs cap layer. The  $\text{Al}_{0.15}\text{Ga}_{0.85}\text{As}$  layers provide a barrier to prevent the diffusion of the charge carriers toward the surface, where they would recombine nonradiatively. The capping layer grown on top on the QDs was kept as thin as possible in order to maximize the evanescent coupling to the WGM. The sample was furthermore processed by electron-beam lithography and reactive ion etching so as to define an array of  $4 \times 4 \mu\text{m}$  micromesas about 200 nm in height, 40  $\mu\text{m}$  apart from one another.

Microphotoluminescence experiments have been performed in order to characterize this QD array, under pumping by a focused laser diode at  $\lambda_{\text{pump}} = 778 \text{ nm}$  (1.59 eV) with a flux of typically  $10^3 \text{ W/cm}^2$ . At room temperature, the QD array exhibits a broad emission line centered at  $\lambda_{\text{PL}} = 1075 \text{ nm}$  (1.15 eV). Its linewidth at half maximum of 100 nm (110 meV) is mainly due to the inhomogeneous broadening resulting from size dispersion, while homogenous broadening due to phonon scattering is known to be about 2.5 THz (10 meV) at 300 K [28]. At 8 K on the opposite, the QD emission spectrum consists of a series of sharp lines, being each related to the emission of one specific QD, under low excitation conditions. Using this feature, we determine the number  $\mathcal{N}$  of QDs per mesa ( $\mathcal{N} \simeq 600$ ) as well as their spectral distribution for the mesas of interest.

## 2.3. Experimental setup

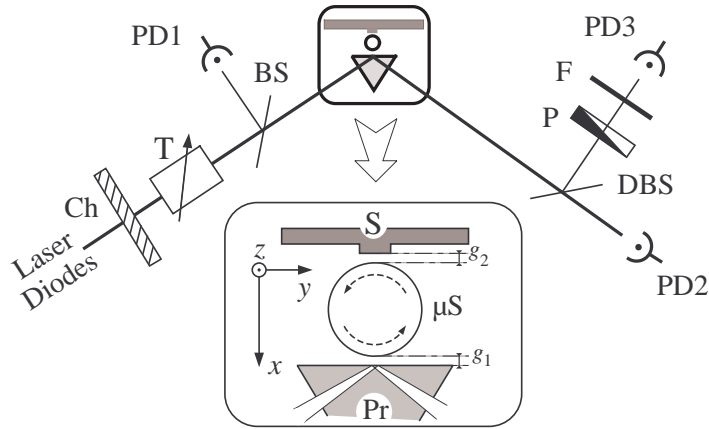


Fig. 1. Scheme of our experimental setup.  $\mu\text{S}$ : Microsphere;  $\text{Pr}$ : coupling prism;  $\text{S}$ : sample;  $\text{Ch}$  : chopper;  $\text{T}$  : attenuator;  $\text{BS}$  : beam-splitter;  $\text{DBS}$  : dichroic beam-splitter;  $\text{P}$ : polarization analyzer;  $\text{F}$ : Wratten 87C or Schott RG1000 filter. Bottom inset: WGM coupling geometry, showing the excitation prism  $\text{Pr}$ , the spherical microcavity  $\mu\text{S}$  and the sample  $\text{S}$ .

The experimental setup is sketched in Fig. 1. Its main features have been described in previous work (see e.g. Ref. [20]). The main advantage of prism-coupling over alternative techniques is the ability to optimize input coupling of the pump while keeping good output coupling of the photoluminescence (PL).

In our experiment, the sphere is placed between the prism and the GaAs sample. This configuration has several key advantages: The pumping laser at  $\lambda_{\text{pump}} \sim 780$  nm is coupled resonantly to a WGM ensuring that only the QDs actually coupled to it can be excited, and the PL extracted through the prism has necessarily been emitted inside the WGMs. The drawback is that the microsphere is almost stuck between two millimeter-sized objects which makes more difficult the overall alignment. The parallelism of the sphere's stem with respect to the prism and the sample is of course crucial in order to prevent any unwanted contact. One also has to control independently the two coupling gaps:  $g_1$  between prism and sphere, and  $g_2$  between the sphere and the sample (top of mesa), as shown in the inset of Fig. 1. Our setup is designed to provide control over the overall 18 degrees of freedom with the necessary precision, using micrometer screws and piezoelectric transducers (PZT).

We have used three different laser diodes for this experiment. Beside the pump laser, two DBR laser diodes operating at  $\lambda_1 = 772$  nm and  $\lambda_2 = 1,060$  nm were used to characterize the prism-sphere and sphere-sample coupling parameters at both the pumping and the emission wavelengths, and to measure the cold cavity linewidth.

#### 2.4. Sphere-Sample coupling optimization

Positioning a given mesa in the field of a strongly confined WGM is absolutely critical. A rough alignment of the setup with a given mesa is first achieved using a stereomicroscope, as shown in the inset of Fig. 2, but visual inspection does not work for further optimization. In order to PZT control the positioning of the selected mesa with desired precision, we monitor the influence of the mesa directly on the WGM resonance signal (amplitude, shift and broadening).

We indeed observe significant sample-induced broadening of the WGM resonances, but no more than the usual broadening due to the prism. With a simple model describing the perturbation induced by a plane dielectric sitting in WGM evanescent field, we have shown (see Ref. [29, 30]) that this modification is characterized by the Fresnel reflection coefficient for the evanescent wave which for TE modes writes:

$$r \approx \frac{i\sqrt{N_{\text{eff}}^2 - 1} - \sqrt{N_D^2 - N_{\text{eff}}^2}}{i\sqrt{N_{\text{eff}}^2 - 1} + \sqrt{N_D^2 - N_{\text{eff}}^2}}, \quad (1)$$

where  $N_{\text{eff}}$  is the WGM effective index, and  $N_D$  the (eventually complex) index of the dielectric. This reflection coefficient accounts for a frequency shift proportional to the real part of  $r$ , and a line broadening proportional to its imaginary part. With  $N_{\text{eff}} \approx N \approx 1.45$  and  $N_D \approx 1.76$  for SF11 or  $N_D \approx 3.36$  for GaAs (at 1,060 nm), one gets  $r \approx 0.05 + i0.999$  for the prism, and  $r \approx 0.77 + i0.63$  for GaAs. This means that, while the index of SF11 gives an almost vanishing shift and a large broadening, the high index of GaAs mainly results in a large shift and a rather moderate broadening [31]. We have experimentally confirmed these predictions by using a flat (un-etched) pure GaAs sample.

As an example of our positioning method, Fig. 2 shows the records obtained when scanning the position of the mesa in a direction  $y$  approximately parallel to the equator, with the gaps ( $x$ ) and the height ( $z$ ) kept constants (see Fig. 1 for definition of axes). The exponential behavior of the evanescent wave results in a Gaussian dependance  $\exp(-\kappa y^2/a)$  of intensity versus  $y$ , where  $\kappa \simeq (N_{\text{eff}}^2 - 1)^{1/2} 2\pi/\lambda$ . Because the height of the mesa is larger than  $\kappa^{-1}$ , and its width larger than the transverse field extension  $(a/\kappa)^{1/2}$ , the mesa can be seen in a first approximation as a small area sample. The behavior of the width or the shift of the line thus appears as a convolution of the square mesa profile and the gaussian, with an expected full width at half maximum of about 5  $\mu\text{m}$ , in good agreement with the experimental results [32]. Due to a slight tilt (about 0.5°) between the sphere axis and the vertical axis  $z$ , the best coupled mode was a mode with  $m = \ell - 7$ . The records obtained for this mode when  $z$  is scanned (not shown here)

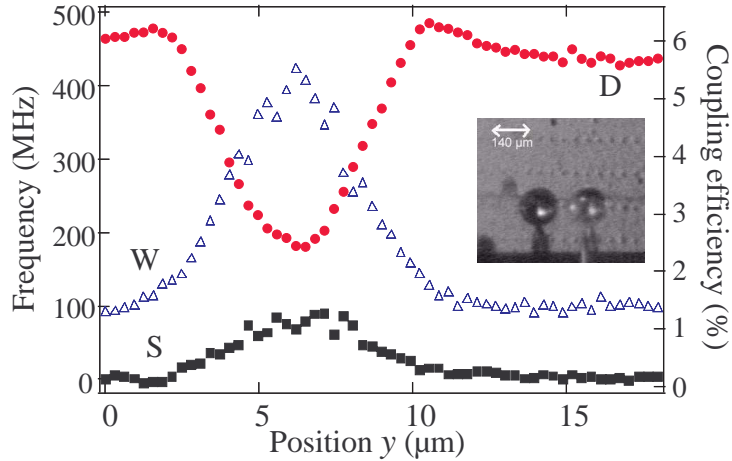


Fig. 2. Evolution of the width (■), shift ( $\triangle$ ) and coupling (●) when the sample is scanned along  $y$ . Inset : Photograph of the sphere in front of the GaAs sample. The sphere is on the right and the image to the left is its reflection in GaAs. The small dots are the  $4\text{ }\mu\text{m} \times 4\text{ }\mu\text{m}$  mesa, revealed by grazing illumination.

actually reveal two antinodes of the polar intensity distribution. In these scans, the observed shift/broadening ratio of 28% is much smaller than the expected value of 78%, as given by Eq. 1. This reveals an extra loss mechanism attributed to the strong light scattering at the edges of the mesa, which will be taken into account below to estimate the pumping efficiency.

### 3. Laser operation

The pump laser used to achieve QD lasing was a widely tunable Littman-Metcalf extended cavity laser diode (Newport/EOSI 2010) with a central wavelength of about 780 nm. Special care had to be taken to filter out a small luminescence from this laser-diode in the 900–1,100 nm range. This parasitic signal which otherwise would hide the QD's emission was eliminated thanks to an additional dispersion prism inserted at the exit of the pump laser.

The QDs emission, outcoupled from the WGMs via the prism Pr, was monitored using an In-GaAs photodiode (Hamamatsu G3476-10) providing sensitivity at the pW level (PD3 in Fig. 1). To extract the PL signal from the noise, the pump beam was chopped at a frequency of about 200 Hz, and a lock-in amplifier was used. We also inserted in front of PD3 three sheets of gelatine IR filter (Kodak Wratten 87C) to further eliminate the residual pump light.

The pump laser was tuned to a strongly confined WGM providing a resonant enhancement of the pumping field chosen to maximize the coupling efficiency. The observed shift/broadening ratio indicates that about one third of the pump power contributes to photoexcitation of the sample (above the bandgap of GaAs).

The sphere–prism and sphere–sample gaps ( $g_1$  and  $g_2$  respectively) also have to be optimized. Because the QDs active medium–field coupling and the resonance broadening exhibit the same exponential behavior, there is *a priori* no preferred  $g_2$  value for laser operation. However, a simple model taking into account the losses due to the prism shows that the lowest threshold should be obtained when  $g_2 = 0$ . We therefore worked with the sample in contact with the sphere, a situation which furthermore provides much better mechanical stability. The gap  $g_1$  was set close to critical coupling for the cavity loaded by the sample. In this situation, the measured cold-cavity width of the best coupled WGMs at 1,060 nm was  $\Gamma/2\pi = 1\text{ GHz}$ .

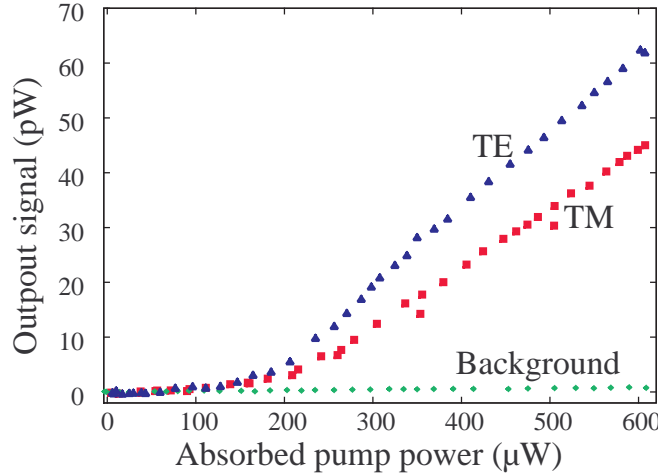


Fig. 3. Emission vs. absorption laser characteristics. The background curve shows the residual fraction of pump laser PL at wavelength higher than 900 nm.

With these settings it was possible to observe the onset of lasing, hallmark by a well pronounced threshold in the pump/emission characteristics curve of the microsphere cavity. Figure 3 shows such a laser characteristic curve for both TE and TM polarization, with a threshold of  $200 \mu\text{W}$ , the lowest observed. In this figure, the “output signal” is the raw detected signal, not corrected for collection and detection efficiency. The “absorbed pump power” is the power lost from the incident beam into the sphere (including scattering) as monitored by photodiodes PD1/PD2 in Fig. 1. These curves were obtained for a  $140 \mu\text{m}$  sphere, pumped into a  $n = 1$ ,  $m = \ell - 6$ , TE polarized WGM.

Due to the small extracted power, and the lack of a low-noise cooled spectroscopic camera, it was not possible to record a spectrum of this laser. However when inserting an additional sheet of Wratten filter or a RG1000 filter we observe a very weak attenuation which demonstrates that the wavelength of the emitted light is 1,000 nm or higher.

Since the coupling of the mesa to the sphere was maximal for a WGM with  $n = 1$  and  $m = \ell - 6$ , the lasing modes also have  $n = 1$  and  $\ell - |m| \approx 6$  providing the best overlap with the mesa. The  $\ell$  value is not limited by the same overlap constraints, and can a priori cover the gain spectral range, hence leading to  $\ell$  values lying between 550 and 600. Multimode operation is therefore very likely, in spite of mode competition.

#### 4. Discussion

##### 4.1. Pumping efficiency

We first discuss the pumping rate achieved in our system. The pumping efficiency is strongly limited by several phenomena. We first take into account the pumping efficiency reduction to about 30% due to the scattering effect revealed by the shift/broadening ratio. Besides, the power actually injected in the sample is absorbed on a characteristic length of about  $1 \mu\text{m}$ , whereas the useful zone between the AlGaAs barriers is only  $70 \text{ nm}$  thick : this introduces an additional factor of 7%, resulting in an overall efficiency of about 2%. An absorbed pumped power of  $200 \mu\text{W}$  therefore corresponds to about  $15 \times 10^{12}$  electron-hole pairs per second. When trapped in a QD, these electron-hole pairs have a total lifetime of about 100 ps at room temperature. This shows the absorbed pump power is large enough to feed the  $\mathcal{N} \approx 600$  QDs in a mesa.

#### 4.2. Threshold condition

The experimental parameters of our system can be used to discuss the lasing threshold condition for a given WGM. The average photon number at threshold  $n^{(\text{th})}$  verifies:

$$n^{(\text{th})} = \mathcal{N}_c^{(\text{th})} \frac{W}{\Gamma} \approx 1 \quad \Rightarrow \quad \mathcal{N}_c^{(\text{th})} \frac{\Omega_R^2}{\gamma_{\text{hom}} \Gamma} \approx 1, \quad (2)$$

with  $\mathcal{N}_c$  the number of QDs coupled to the mode,  $W$  the spontaneous emission rate in the mode and  $\Gamma/2\pi$  the WGM's linewidth. Here the second equality results from  $W = \Omega_R^2/\gamma_{\text{hom}}$ , with  $\Omega_R$  denoting the vacuum Rabi frequency and  $\gamma_{\text{hom}}/2\pi$  the homogenous linewidth [25]. In the experiment discussed here the WGM mode volume is about  $5,000 \mu\text{m}^3$  in the lasing wavelength range, leading to a maximal Rabi frequency  $\Omega_R/2\pi \approx 2 \text{ GHz}$  at the point where the WGM's field reaches its maximum  $E_{\text{max}}$ .

Using the above mentioned parameters, we are left with the frequency hierarchy:

$$\frac{\gamma_{\text{inh}}}{2\pi} \approx 25,000 \text{ GHz} \gg \frac{\gamma_{\text{hom}}}{2\pi} \approx 2,500 \text{ GHz} \gg \frac{\Delta\omega_{\text{FSR}}}{2\pi} \approx 500 \text{ GHz} \gg \frac{\Gamma}{2\pi} \approx 1 \text{ GHz} \quad (3)$$

for the QD's inhomogeneous width, the QD's homogenous width, the WGM's free spectral range and the WGM linewidth, respectively.

As stated above, the recombination emission of the  $\mathcal{N}$  QDs is spread over a frequency span  $\gamma_{\text{inh}}/2\pi$ , which encompasses about 50 FSR. Inside a  $\gamma_{\text{hom}}/2\pi$  frequency bandwidth, mode competition is expected to favor one lasing mode. Such a mode interacts resonantly with  $\mathcal{N}_c \approx \mathcal{N} \gamma_{\text{hom}} / \gamma_{\text{inh}} \approx 60$  QDs.

Considering the critical parameter  $\Omega_R^2/\gamma_{\text{hom}}\Gamma$  which enters Eq. 2, it is of the order of  $1.6 \times 10^{-2} \times (E_{\text{QD}}/E_{\text{max}})^2$ . The threshold condition can be fulfilled if the ratio  $(E_{\text{QD}}/E_{\text{max}})^2$  is close enough to 1. This condition suggests that the WGM field in the coupling zone is deconfined from the sphere to the high index sample. We believe that this reconstruction mechanism explains our observations when studying different mesas: although they show the same PL characteristics, some lase while others do not, everything else being equal. Indeed the mode reconstruction, which depends on the precise size and structure of the mesa, is expected to vary from one mesa to the other.

To summarize, the orders of magnitude discussed above are consistent with an absorbed pump power of  $200 \mu\text{W}$  at threshold sustaining about 10 modes with 60 active QDs per mode.

## 5. Conclusion

We have successfully combined the high quality factor of the WGM in a microsphere, the large oscillator strength of III-V semiconductor QDs to achieve room-temperature lasing with less than 100 QDs per mode. This result clearly demonstrates the potential of high- $Q$  WGM microcavities coupled to semiconductor nanostructures, a combination which is expected to gain further applications in the near future.

## Acknowledgements

The authors warmly thank Jean-Michel Raimond and Serge Haroche for fruitful and encouraging discussions. JMG gratefully thanks B. Gayral and Y. Nowicki for the characterisation of the QD sample by microphotoluminescence. Laboratoire Kastler Brossel is a laboratory of École normale supérieure and Université P.&M. Curie, associated to C.N.R.S. (UMR 8552). This work was partly supported by CNRS-Japan Science and Technology contract (Stanford/Ens ICORP “Quantum Entanglement” Project) and by European Community (QUBITS Network).